

Article

Synthesis and Characterization of Crown-Ether Appended Hexaazatrinaphthylene-Based Liquid-Crystalline Derivative

Kyosuke Isoda ^{1,2,*}  and Keigo Shimooka ¹

¹ Faculty of Engineering and Design, Kagawa University, 2217-20 Hayashi-cho, Takamatsu, Kagawa 761-0396, Japan; s18g564@stu.kagawa-u.ac.jp

² Health Research Institute, National Institute of Advanced Industrial Science and Technology (AIST), 2217-14 Hayashi-cho, Takamatsu, Kagawa 761-0395, Japan

* Correspondence: k-isoda@eng.kagawa-u.ac.jp; Tel.: +81-87-864-2395

Received: 19 March 2020; Accepted: 29 April 2020; Published: 7 May 2020



Abstract: In this article, we report on the synthesis and characterization of crown-ether appended hexaazatrinaphthylene derivatives with two alkoxy chains. The complexation of a derivative having shorter alkoxy chains with metal ions, such as NaI and KI, prompts remarkable changes in the electronic properties of solid states, because of changing intermolecular interactions. Polarized optical microscopic observation, X-ray diffraction pattern measurement and differential scanning calorimetry reveal that a compound with longer alkoxy chains self-assembles into the formation of the columnar liquid-crystalline phase. Moreover, the addition of benzenesulphonic acid influences the self-assembled liquid-crystalline structures, as well as the electronic properties. The complexation of the derivative having longer alkoxy chains with benzenesulphonic acid induces a larger dipole moment, compared to that before complexation, thereby leading to the enhancement of intermolecular interaction, such as dipole-dipole interaction. Also, peaks in UV-vis absorption and fluorescent spectra show a dramatically bathochromic shift, due to their intermolecular interaction, such as the π - π interaction.

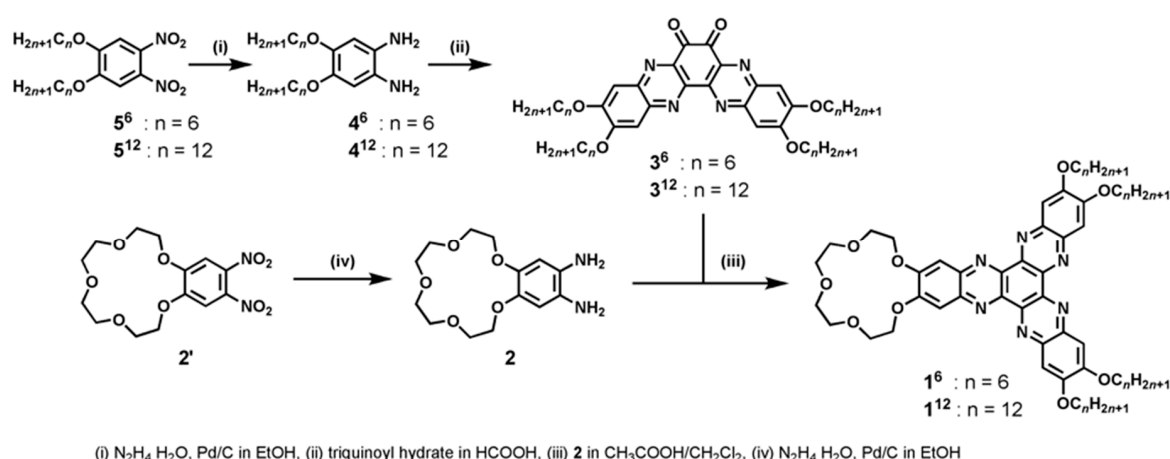
Keywords: liquid crystals; stimuli response; hexaazatrinaphthylene; electron acceptor

1. Introduction

Discotic molecules have gained much attention as the building blocks for the development of one-dimensional self-assembled structures in solid-state materials [1–5]. Among them, disc-like molecules, such as triphenylene and benzocoronene derivatives, are well known as representative π -conjugated frameworks, composed of planar polyaromatic hydrocarbon with C_3 symmetry. The substitution of flexible alkyl chains into these π -conjugated frameworks plays a role to self-assemble into one-dimensional columnar liquid-crystalline structure transporting charge carriers such as hole and electron along to the column axis. Also, their electronic properties can be tuned by the incorporation of heteroatoms, such as N atoms, of which its derivatives are called hexaazatriphenylene, hexaazatrinaphthylene and azacoronene. As hexaazatriphenylene- and hexaazatrinaphthylene-based materials are composed of electron-deficient pyrazine units, it is known that they can transport a charge carrier as an electron along to the column axis in the columnar liquid-crystalline phase [6–9]. In particular, some groups have used the hexaazatrinaphthylene framework as an excellent building block to fabricate the organic functional materials, because of its physicochemical potential. For example, liquid-crystalline hexaazatrinaphthylene-based materials have been reported as having the potential for charge-transporting properties, elucidated in experimental and theoretical studies by

Brédas, Cornil and Crispin et al. [6,7], facile synthesis by Ong et al. [10,11], liquid-crystalline behaviors and carrier mobility by Lehmann et al. [8,9], as well as Marder et al., who have shown it also has a high charge-carrier mobility in amorphous state [12]. Recently, the uses of the hexaazatriphthylene framework have been expanded in the field of solid-state materials for nanoporous structures, such as covalent organic frameworks and hydrogen-bonded organic frameworks. McKeown et al. have reported potential as adsorbent and catalyst support for covalent organic frameworks based on hexaazatriphthylene [13,14]. Other groups have reported hexaazatriphthylene-based covalent organic frameworks showing redox-active behavior and [15] heavy metal removal and photoredox catalysis [16]. Hisaki et al. have reported hexaazatriphthylene-based hydrogen-bonded organic frameworks in response to acid [17]. Furthermore, the combination of other functional moieties into the HATN framework are expected to promote the creation of novel functional materials.

Based on this concept, in this study, we report on the incorporation of crown-ether moiety as a functional moiety in the hexaazatriphthylene framework, to show its multi-functionalities in Scheme 1. Compounds **1**⁶ and **1**¹² consist of hexaazatriphthylene, having four alkoxy chains with hexyl and dodecyl, respectively, and crown-ether moiety at terminal. As crown-ether is a well-known macrocyclic compound, which can capture with alkali metal ion and transport metal ion, [18] compounds **1** are expected to form one-dimensional columnar liquid-crystalline structures, in which columns have the potential to transport both electron and metal ion. Also, we focus on the acid-responsive properties of **1** for metal ion, as well as acid substances. Crown-ether moiety of **1** is weakly polar, because polar oxygen atoms at the inner positions are surrounded by nonpolar ethylene moieties at the outer positions, whereas capturing metal ion can induce a polarity, due to existence of counter anions. Additionally, since the imino-N atom in pyrazine works as a Lewis base, the interaction with Lewis acid added leads to the tuning of physicochemical properties, such as fluorescent and electronic properties, as well as intermolecular interaction with one another in solid states [19–24]. Accordingly, **1** designed as a nonpolar derivative has a potential to turn into polar derivative by the complexation of metal ions, as well as Lewis acid, which is expected to affect the electronic properties and structures, as well as the thermal stability of the self-assembled structures. To the best of our knowledge, this is the first report on crown-ether appended hexaazatriphthylene.



Scheme 1. Synthesis of compounds **1**⁶ and **1**¹².

In this article, at first, we demonstrated how the complexation with metal ions influences the electronic properties of **1**⁶ with shorter alkoxy chains in solution and solid state. Then, we investigated self-assembled structures and electronic properties of **1**¹² with longer alkoxy chains in solution and liquid-crystalline states.

2. Materials and Methods

^1H and ^{13}C NMR spectra were recorded on a Varian UNITY INOVA400NB spectrometer (Varian, Palo Alto, CA, USA). The chemical shift of the ^1H and ^{13}C NMR signals were quoted as tetramethylsilane ($\delta = 0.00$) and ($\delta = 77.00$) as internal standards, respectively. FT-IR spectra were measured with a Perkin-Elmer Spectrum Two FT-IR Spectrometer (Perkin Elmer, Waltham, MA, USA). Matrix-assisted laser desorption/ionization time-of-flight (MALDI-TOF) mass spectra were collected on a JEOL JMS-S3000 instrument (JEOL, Tokyo, Japan), using dithranol as a matrix. UV-vis absorption spectra were recorded with a Perkin-Elmer Lambda35 UV-vis Spectrometer (Perkin Elmer, Waltham, MA, USA). Fluorescent spectra were recorded with a Perkin-Elmer LS45 Luminescence Spectrophotometer (Perkin Elmer, Waltham, MA, USA). Cyclic voltammetry was carried out in CH_2Cl_2 solution of Bu_4NPF_4 (0.10 M) with a glassy carbon working, Pt counter, and an Ag/Ag^+ reference electrode using an ALS CHI 600E electrochemical analyzer (ALS Co., Ltd., Tokyo, Japan). XRD patterns were obtained at room temperature using a Rigaku Rapid II diffractometer, using Ni-filtered $\text{Cu}\alpha$ radiation (RIGAKU, Tokyo, Japan). Differential scanning calorimetry (DSC) measurements were performed on a NETZSCH DSC 200 F3 Maia at a scanning rate of $10\text{ }^\circ\text{C min}^{-1}$ (NETZSCH, Deutschland, Germany). Polarized optical microscopic observations were performed on a Nikon OPTIPHOT-POL polarized optical microscope equipped with Mettler FP82 HT hot stage. Density functional theory calculations were carried out using the Wavefunction Inc. SPARTAN'16 suite of programs (Wavefunction, Inc., Irvine, CA, USA). Ground-state geometries were optimized at the B3LYP/6-31G* level of theory [25–27]. All reagents and solvents were purchased from FUJIFILM Wako Pure Chemical Corporation (Osaka, Japan), Tokyo Chemical Industry Co., Ltd. (Tokyo, Japan), Kanto Chemical Co. (Tokyo, Japan), Inc., or Sigma-Aldrich Co. LLC, and used as received. Compounds **2** and **3** were prepared according to the procedures of the literature [28,29].

2.1. Synthesis of **1**¹²

To a suspension of **4**¹² (4.04 g, 8.0 mmol) and Pd/C (0.50 g) in dry EtOH (150 mL) at $0\text{ }^\circ\text{C}$ was added dropwise hydrazine monohydrate (4.0 mL). After reflux for 24 h, the reaction mixture was filtrated through Celite under Ar, and then evaporated. The crude product was reacted with triquinoyl hydrate (0.47 g, 2.8 mmol) in HCOOH (50 mL) at r.t. under Ar for 2.5 h. The reaction mixture was extracted with CHCl_3 three times. The combined organic layers were washed with water, and dried over anhydrous Na_2SO_4 to obtain a red solid. The reaction mixture was heated with **2** (prepared by using **2'** (0.90 g, 2.5 mmol), Pd/C (0.50 g), hydrazine monohydrate (4.0 mL) in dry EtOH (50 mL) according to the procedure of **4**¹²) in AcOH (50 mL) and CH_2Cl_2 (50 mL) at $50\text{ }^\circ\text{C}$ under Ar for 24 h. After cooling to r.t., the reaction mixture was extracted with CHCl_3 three times, washed with H_2O , and dried over anhydrous Na_2SO_4 . After filtration and evaporation, the crude product was purified by column chromatography (silica, CHCl_3 and $\text{CHCl}_3/\text{MeOH} = 20/1$ (v/v)), and dried under vacuum to afford **1** as a yellow solid (0.43 g, 11.7% in 4 steps). IR (ATR): $\nu = 2921, 2842, 1505, 1235, 842, 730\text{ cm}^{-1}$; ^1H NMR (400 MHz, CDCl_3): δ 7.86 (s, 2H), 7.85 (s, 2H), 7.84 (s, 2H), 4.40 (m, 4H), 4.31–4.30 (m, 8H), 4.07 (m, 4H), 3.86 (m, 8H), 2.00 (m, 8H), 1.60–1.55 (m, 24H), 1.40–1.25 (m, 48H), 0.89–0.87 (m, 12H) ppm; ^{13}C NMR (75 MHz, CDCl_3): δ 154.55, 154.52, 154.16, 141.58, 141.36, 141.31, 141.14, 141.02, 140.86, 107.69, 107.63, 107.61, 71.35, 70.14, 69.49, 68.94, 68.66, 68.65, 31.92, 29.70, 29.66, 29.63, 29.40, 29.37, 28.78, 26.07, 22.68, 14.11. ppm; MS (MALD-TOF-MS): m/z calcd: 1311.86 [M]⁺; found: 1312.31; elemental analysis: calcd (%) for $[\text{C}_{80}\text{H}_{118}\text{N}_6\text{O}_9]$ (CHCl_3)_{0.5}: C 70.49, H 9.00, N 6.13; found: C 70.92, H 9.40, N 6.07.

2.2. Synthesis of **1**⁶

To a suspension of **4**⁶ (1.85 g, 5.0 mmol) and Pd/C (0.30 g) in dry EtOH (60 mL) at $0\text{ }^\circ\text{C}$ was added dropwise hydrazine monohydrate (3.0 mL). After reflux for 24 h, the reaction mixture was filtrated through Celite under Ar, and then evaporated. The crude product was reacted with triquinoyl hydrate (0.34 g, 2.0 mmol) in HCOOH (50 mL) at r.t. under Ar for 2.5 h. The reaction mixture was

extracted with CHCl_3 three times. The combined organic layers were washed with water, and dried over anhydrous Na_2SO_4 to obtain a red solid. The reaction mixture was heated with **2** (prepared by using **2'** (0.36 g, 1.0 mmol), Pd/C (0.50 g), hydrazine monohydrate (4.0 mL) in dry EtOH (50 mL), according to the procedure of **4**⁶) in AcOH (50 mL) and CH_2Cl_2 (50 mL) at 50 °C under Ar for 24 h. After cooling to r.t., the reaction mixture was extracted with CHCl_3 three times, washed with H_2O , and dried over anhydrous Na_2SO_4 . After filtration and evaporation, the crude product was purified by column chromatography (silica, CHCl_3 and $\text{CHCl}_3/\text{MeOH} = 20/1$ (v/v)), and dried under vacuum, to afford **1** as a yellow solid (0.18 g, 9.2% in 4 steps). IR (ATR): $\nu = 2932, 2865, 1494, 1438, 1224, 1157, 853, 561 \text{ cm}^{-1}$; ^1H NMR (400 MHz, CDCl_3): δ 7.86 (s, 2H), 7.85 (s, 2H), 7.84 (s, 2H), 4.41 (m, 4H), 4.31 (m, 8H), 4.08 (m, 4H), 3.85 (m, 8H), 2.00 (m, 8H), 1.42 (m, 24H), 0.96 (m, 12H) ppm; ^{13}C NMR δ 154.51, 154.48, 154.11, 141.32, 141.28, 141.26, 141.12, 141.00, 140.84, 107.69, 107.60, 107.59, 71.34, 70.13, 69.45, 68.92, 68.64, 31.54, 28.73, 25.71, 22.58, 13.98. ppm MS (MALD-TOF-MS): m/z calcd: 975.22 $[\text{M}]^+$; found: 975.85; elemental analysis: calcd (%) for $[\text{C}_{56}\text{H}_{74}\text{N}_6\text{O}_9] (\text{CHCl}_3)_{0.5}$: C 65.57, H 7.26, N 8.12; found: C 65.49, H 7.95, N 8.04.

3. Results and Discussion

3.1. Synthesis and Characterization of Compounds **1**⁶ and **1**¹²

We have synthesized compounds **1**⁶ and **1**¹², according to the previous procedure in Scheme 1 [11,28]. Compound **3** was prepared by the reduction of **4** with $\text{N}_2\text{H}_4 \cdot \text{H}_2\text{O}$ and Pd/C in EtOH, which was used to react with triquinoyl hydrare without further purification, because **3** was too air-sensitive to be purified. This reaction condition can preferentially provide di-substituted derivative, whereas mono- and tri-substituted derivatives are scarcely obtained, which is consistent with results reported by Ong et al. [11]. Then, the reaction mixture including **3** was reacted with compound **2** and purified by column chromatography twice, to afford compound **1** as a brown solid, as demonstrated by NMR analysis reported in Figures S1 and S2 in Supplementary Materials. The cyclic voltammetry of **1**¹² shows three consecutive reduction peaks, derived from the formation of radical anion, dianion and trianion, respectively, in Figure 1. **1**⁶ showed the same behavior as **1**¹², indicating that **1**⁶ and **1**¹² have the potential to function as an electron acceptor, as well as electron-transporting materials.

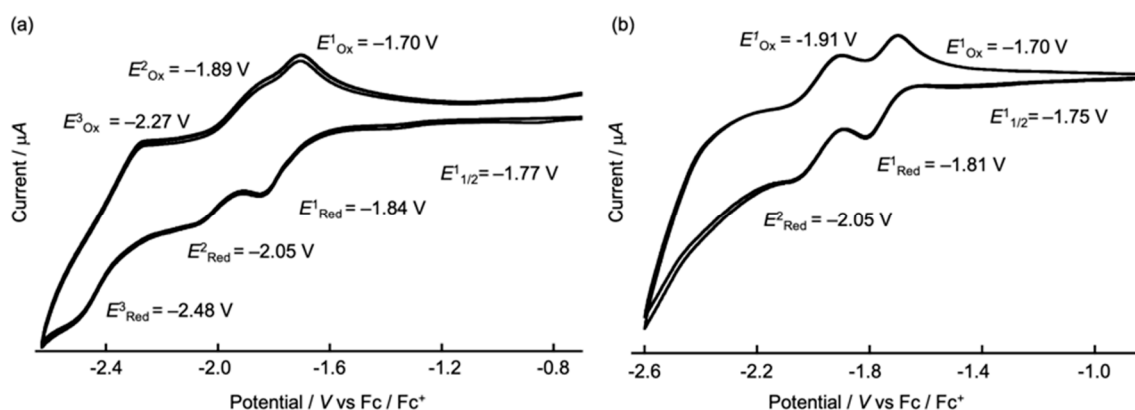


Figure 1. Cyclic voltammetry of 1.0 mM for **1**¹² (a) and **1**⁶ (b) in a 0.10 M solution of Bu_4NPF_6 in CH_2Cl_2 at a scanning rate of 100 mVs^{-1} .

3.2. Influence on Self-Assembled Liquid-Crystalline Structures of **1**¹² by Addition of BSA and Metal Ions

To investigate the LC properties, we carried out polarized optical microscopic (POM) observations, differential scanning calorimetry (DSC), and X-ray diffraction (XRD) measurements. At first, we synthesized **1**⁶ having four alkoxy chains. However, it was not found that **1**⁶ self-assembled into the formation of LC phase by measurements. In order to promote the self-assembling behavior of

this framework, we designed the elongation of alky chains and substituted four hexyl chains with four dodecyl chains. The DSC measurement of **1**¹² did not show a clear peak, due to a phase transition from a liquid-crystalline (LC) phase to an isotropic liquid at a scanning rate of 10 K/min on both first cooling and second heating in Figure 2. On the other hand, the POM observation in Figure 3 reveals that **1**¹² shows a clearing point from a LC phase to isotropic liquid at 114 °C on the first heating. On the first cooling, annealing for 30 min at 110 °C brings about the formation of the LC phase in Figure 3. When the LC film of **1**¹² applied into a sandwiched glass cell is sheared, this LC film can be aligned along to the shearing direction in Figure 3. POM observations reveal that the sheared LC film shows a bright and a dark image by 45° rotation. These observations indicate that **1**¹² self-assembles into the formation of columnar (Col) LC phase, in which sheared columns are homogeneously aligned parallel to a glass cell. DSC and POM observation results indicate that **1**¹² shows Col LC phase in a wide temperature range, including room temperature. Ong et al. have reported Col LC materials based on the similar HATN framework, which are composed of four alkoxy chains, as well as two triethylene glycol monomethyl ether chains [11]. Also, a glass transition of **1**¹² are observed at −35 °C, according to the peak, due to phase transition from a Col LC state to a glass state in Figure 2. The XRD pattern of **1**¹² shows two peaks in a small-angle region, with a broaden peak in a wide-angle region, due to molten alkoxy chains. These peaks can be assigned as the rectangular columnar LC (Col_r) structure with a lattice constant ($a = 48.0 \text{ \AA}$, $b = 41.5 \text{ \AA}$) in Figure 5.

The complexation of compound **1**¹² with benzenesulphonic acid (BSA) or metal ions leads to clear changes in phase transition temperature, as well as self-assembling behavior. Complexes of **1**¹² with BSA can form Col LC phases without annealing. DSC traces in Figure 4 reveal that the LC sample **1**¹²₁₀₀ shows a melting point at 117 °C, which becomes higher than that at 104 °C for **1**. These melting points for complex of **1**¹² with BSA are gradually increasing, accompanied by the additional ratio of BSA relative to **1**¹² in Table 1. As for **1**¹²₁ and **1**¹²₂, decomposition was observed before the melting point on the first heating. Also, phase transition temperatures of complexes from Col to Iso tend to become clear peaks, as well as their enthalpies (ΔH) estimated by DSC results, which gradually rise with increase in the ratio of BSA in Table 1. These results indicate that the complexation of **1**¹² with BSA should influence an enhancement of the intermolecular interaction in the LC phase. To investigate the relationship between complexation and self-assembled structures, we carried out the XRD measurements in Figure 5. It is observed that two peaks for **1** in a small-angle region are merged into one peak, accompanied by increasing ratio of an amount of BSA relative to **1**¹². These results indicate that the addition of BSA should generate the polarity of **1**¹², leading to the formation of more ordered Col structure, strongly showing intermolecular interactions with one another, as compared with **1**¹². Density functional theory (DFT) calculations at the B3LYP/6-31G* level were operated by using SPARTAN'16 package in Figure 6a,b [25–27]. DFT calculation revealed the complexation of **1**¹² with BSA induced larger dipole moment (9.87 Debye) than **1**¹² (5.25 Debye), which should play a driving force to stabilize the Col LC phase. Also, the electrostatic interaction between the protonated **1**¹² and benzenesulphonate anion should stabilize the Col LC structure. This explanation is almost consistent with results for **1**¹²₁ and **1**¹²₂, for which the peak appears at 3.4 Å in a wide-angle region. This peak should be assigned as a π - π interaction, due to the stacking of π -conjugated frameworks with one another in a column. Additionally, the peak, due to d_{100} of **1**¹², tends to become so narrow that relationship between the columns should become ordered by the addition of BSA.

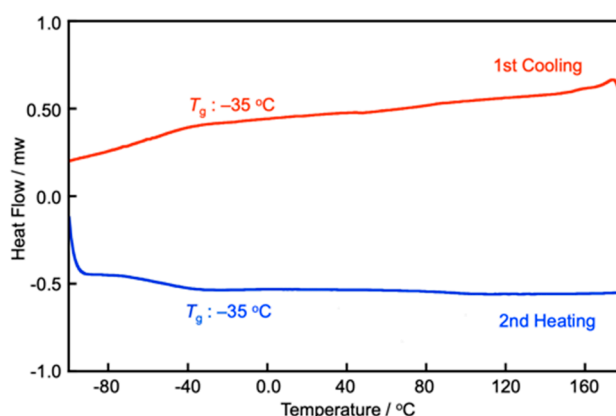


Figure 2. Differential scanning calorimetry (DSC) traces (right) of 1^{12} at the rate of 10 K/min.

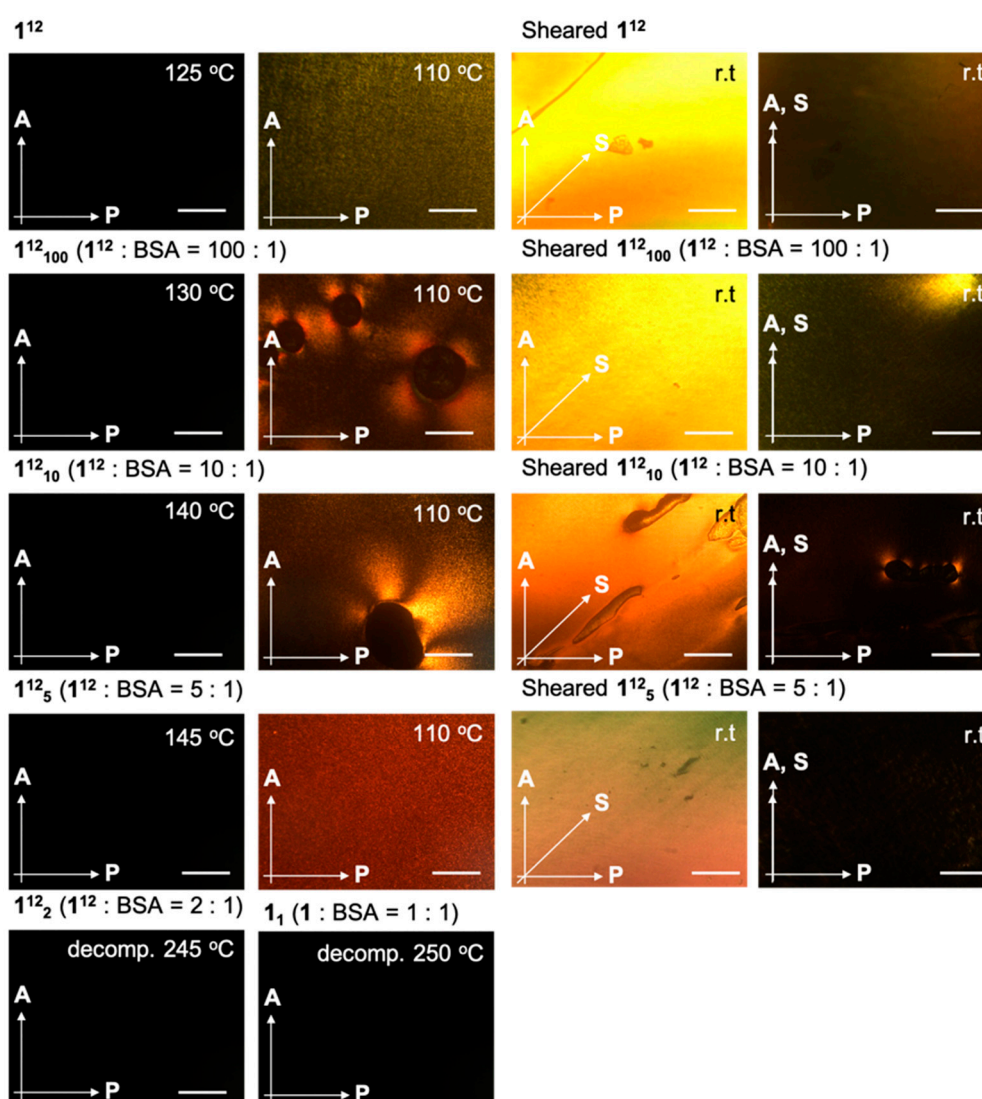


Figure 3. Polarized optical microscopic (POM) observations of 1 and complexes of 1 with benzenesulphonic acid (BSA) for 1^{12}_{100} , 1^{12}_{10} , 1^{12}_5 , 1^{12}_2 , and 1^{12}_1 . All scale bars indicate 100 μm . A, P, and S indicate analyzer, polarizer, and sheared direction, respectively. 1^{12}_{100} , 1^{12}_{10} , 1^{12}_5 , 1^{12}_2 , and 1^{12}_1 indicate 1: BSA = 100:1, 10:1, 5:1, 2:1, and 1:1 (in molar), respectively.

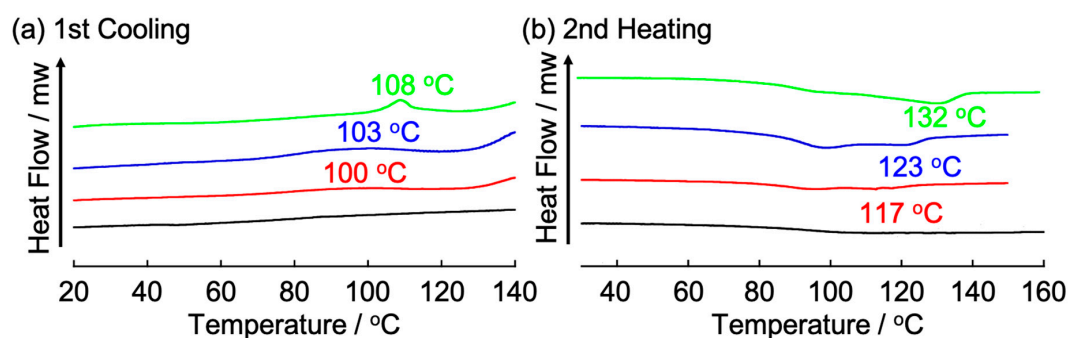


Figure 4. DSC traces of 1^{12} and complexes of 1^{12} with BSA for 1^{12}_{100} , 1^{12}_{10} , and 1^{12}_5 on 1st cooling (a) and 2nd heating (b).

Table 1. Phase transition behavior and d values estimated from XRD for 1^{12} and complexes of 1^{12} with BSA.

| Complex | m.p./°C ^a | Peak Top/°C ^b | ΔH /KJ/mol ^c | Angle (d Value)/° (Å) ^d |
|----------------|----------------------|--------------------------|---------------------------------|--|
| 1^{12} | 114 | – | – | 2.8 (d_{110} 31.4), 3.7 (d_{200} 24.0) |
| 1^{12}_{100} | 121 | 100 | 3.56 | 2.8 (d_{100} 31.4) |
| 1^{12}_{10} | 128 | 103 | 4.34 | 2.8 (d_{100} 31.4) |
| 1^{12}_5 | 140 | 108 | 4.54 | 3.1 (d_{100} 28.7) |
| 1^{12}_2 | 240 (Decomp.) | – | – | 3.2 (d_{100} 27.5) |
| 1^{12}_1 | 250 (Decomp.) | – | – | 3.7 (d_{100} 23.6) |

^a Determined by POM observation; ^{b,c} Determined by DSC traces on 2nd heating; ^d Determined by XRD results.

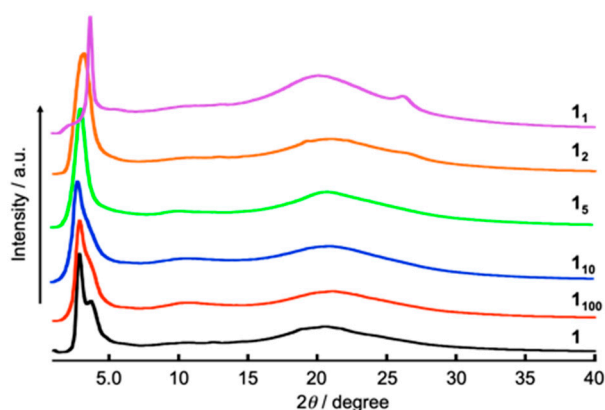


Figure 5. X-ray diffraction (XRD) patterns of 1^{12} and complexes of 1^{12} with BSA for 1^{12}_{100} , 1^{12}_{10} , 1^{12}_5 , 1^{12}_2 and 1^{12}_1 at room temperature.

As for the addition of 1^{12} with Na^+ salt (NaI), which can be captured by 15-crown-5 moiety, we firstly carried out ^1H NMR measurements to confirm the recognized behavior with metal ions by crown-ether moiety in Figure 6. In ^1H NMR spectra for 1^{12} , the addition of NaI leads to an obvious change in the chemical shift and the broadening of the peaks, indicating that the complexation of 1^{12} with NaI should occur. On the other hand, POM observation revealed that complex of 1^{12} with NaI showed no birefringence characteristic of the LC phase, as well as decomposition before the melting point. As for complexation with KI, the broadening of the peaks due to crown-ether moiety was observed, however, the melting point was not changed compared with 1^{12} .

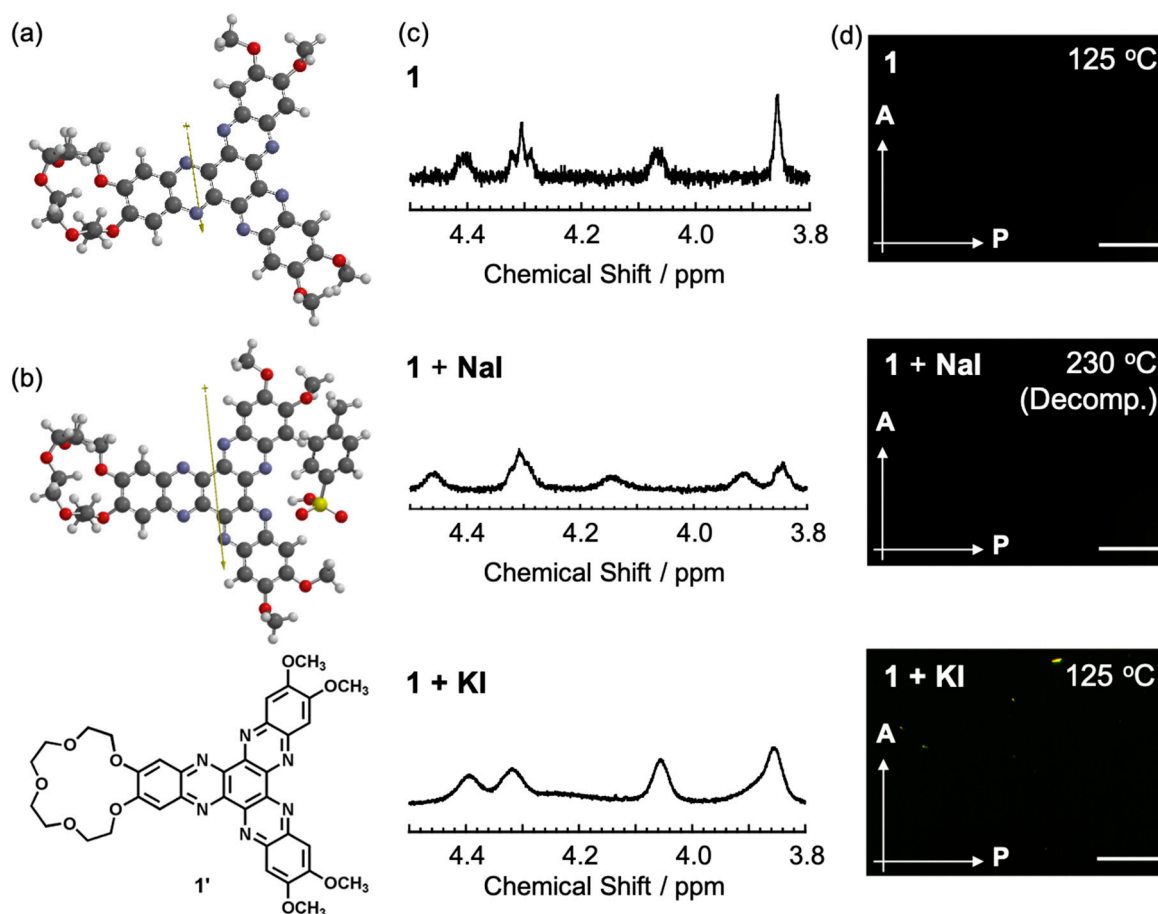


Figure 6. Density functional theory (DFT) calculations by using **1'** (a) and complex **1'** of with BSA (b). Arrows indicate dipole moments. (c) ^1H NMR spectra and of **1**¹² (top) and **1**¹² with NaI (middle) and KI (bottom) in the range of crown-ether moieties and (d) POM observations of **1**¹² (top) and **1**¹² with NaI (middle) and KI (bottom).

3.3. Influence on Electronic Properties of **1**⁶ by Addition of Metal Ions

We carried out the UV-vis and fluorescent (FL) spectra in the solution and solid states to investigate the change in the electronic properties of **1**⁶ by the complexation with metal ions in Figure 7. In the solution states, UV-vis spectra of **1**⁶ showed some peak maxima, whereas the addition of metal ions scarcely brought about clear changes in Figure 7a. As for the FL spectra, similar behavior was observed, indicating that intermolecular interaction should not occur, such as the π - π interaction in experimental conditions in Figure 7b. Additionally, the UV-vis absorption spectrum of **1**⁶ in a solid state was almost the same as that of **1**⁶ in a solution state in Figure 7c, whereas the addition of metal ions brought about changes in Figure 7d. On the other hand, FL spectra of **1**⁶ with yellow emission in a solid state showed remarkable changes, of which peak maxima was bathochromically shifted, compared with **1**⁶ with blue emission in a solution state. This result strongly implied that the π - π interaction between π -conjugated frameworks of **1**⁶ should happen. Further, the addition of metal ions led to clear changes in the FL spectra, as well as in emission colors. Interestingly, the peak at 525 nm for **1**⁶ was hypsochromically shifted to 483 nm for **1**⁶ + NaI, and to 520 nm for **1**⁶ + KI. This result suggested that the addition of metal ions should change the molecular alignments, as well as weakening the intermolecular interactions between the **1**⁶ molecules.

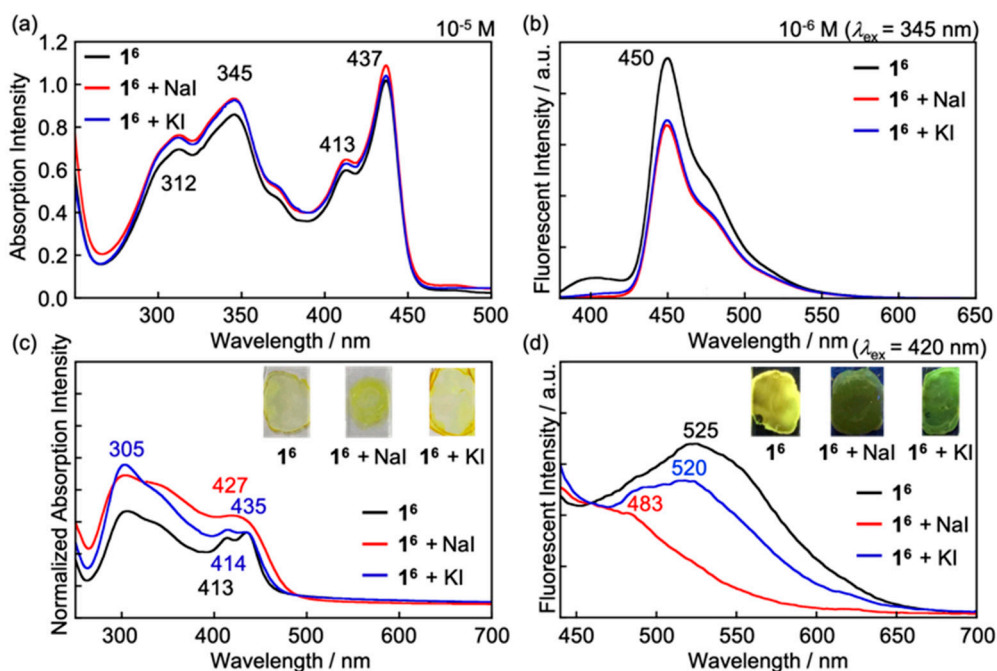


Figure 7. UV-vis absorption spectra and photographs in CHCl_3 solutions (a) and in solid states (c) and fluorescent spectra and photographs in CHCl_3 solutions (b) and in LC states (d) for complexes 1^6 with BSA.

3.4. Influence on Electronic Properties of 1^{12} by Addition of BSA

We carried out UV-vis and FL spectra to investigate influence on electronic properties of 1^{12} by addition of BSA in solution and LC states in Figure 8. UV-vis absorption spectrum of 1^{12} in CHCl_3 solution (10^{-5} M) shows mult peaks, of which peaks are slightly changed by addition of BSA in Figure 8a. On the hand, the new broad peak due to the protonated **1** clearly appears around at 500 nm, which is gradually increased with increasing BSA. FL spectrum of 1^{12} in the CHCl_3 solution (10^{-6} M) shows a peak at 456 nm, of which emission color is light blue in Figure 8b. Upon addition of BSA, a peak shift due to protonation in FL spectra is not observed because 1^{12} would weakly interact with BSA at an excited state in dilute solution states. Therefore, we carried out both measurements in condensed Col LC films without effects of solution molecules. UV-vis absorption spectrum of 1^{12} in the LC film at room temperature shows three peaks with a longest wavelength at 430 nm, which are almost similar to that in the CHCl_3 solution state in Figure 8c. On the other hand, the complexation between 1^{12} and BSA gives the new peak around at 550 nm, which is derived from protonated 1^{12} . Further, wavelengths of absorption edges were bathochromically shifted with increasing the BSA ratio in Figure 8d. These reasons are presumably why stronger π - π stacking leads to narrowing the HOMO-LUMO energy gap. In the FL spectrum, 1^{12} in the LC film shows a peak at 540 nm with emission color of yellow, although the complexation of **1** with BSA clearly shows a red shift of FL peaks, accompanied with the decrease in FL intensities. Also, emission colors for complex of 1^{12} with BSA are gradually changing from yellow (for 1^{12}), orange (for 1^{12}_{100} at 553 nm), to deep orange (for 1^{12}_{10} and 1^{12}_5 at 605 nm). On the other hand, 1^{12}_2 slightly shows photoluminescence at 553 nm, whereas it is observed that 1^{12}_1 scarcely emits in LC films, respectively. As a result, the linear correlation between an amount of BSA and fluorescent peak was very weak. Increasing BSA relative to 1^{12} should promote π - π interaction between π -conjugated framework derived from origin of emission, which should cause self-quenching in condensed states. These explanations are consistent with DSC results on increment of phase transition enthalpy as well as XRD results on appearance of peak at 3.4 \AA for 1^{12}_1 .

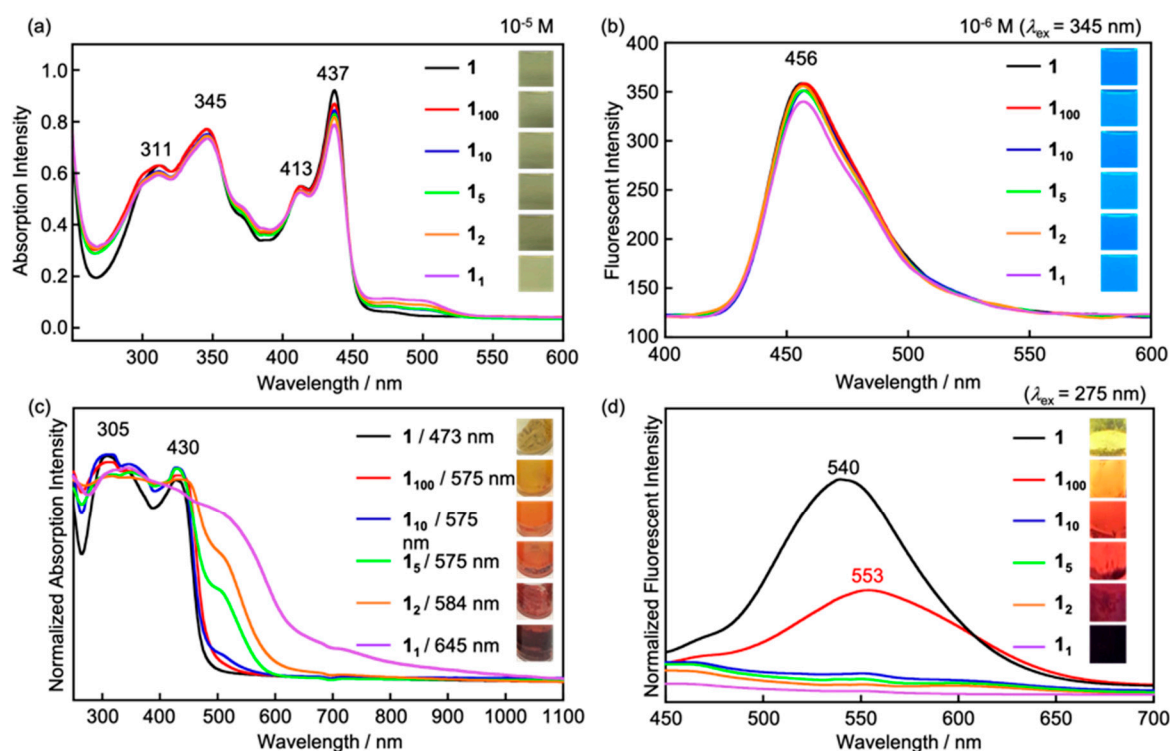


Figure 8. UV-vis absorption spectra and photographs in CHCl_3 solutions (a) and in liquid-crystalline (LC) states (c) and fluorescent spectra and photographs in CHCl_3 solutions (b) and in LC states (d) for complexes 1^{12} with BSA.

4. Conclusions

We synthesized novel crown-ether appended HATN LC material **1** in the first time. Compound **1** functioned as electron acceptor and self-assembled into the Col LC structure. The complexation of 1^6 with metal ions leads to a remarkable change in electronic properties, such as fluorescent colors in solid states, as well as the addition of BSA into 1^{12} , which can tune self-assembled Col LC structures, as well as electronic properties, such as fluorescent colors. In particular, an increasing amount of BSA into 1^{12} leads to the stabilization of the Col LC structures, because of induced dipole moment and electrostatic interactions. This method is expected to be efficient for tuning the electronic properties, as well as self-assembled structures for π -conjugated materials containing nitrogen atoms.

Supplementary Materials: The following are available online at <http://www.mdpi.com/2073-4352/10/5/377/s1>, Figure S1: ^1H NMR and ^{13}C NMR spectra of 1^6 , Figure S2: ^1H NMR and ^{13}C NMR spectra of 1^{12} .

Author Contributions: K.S. synthesized **1** and carried out all experiments. K.I. designed and supervised this project, and wrote the manuscript. All authors have read and agreed to the published version of the manuscript.

Funding: This work was supported by the Japan Society for the Promotion of Science (JSPS) KAKENHI Grant Number 16H04095 and 18K05263, The Murata Science Foundation, the Tokyo Kasei Chemical Promotion Foundation, The Hyakujushi Bank, Academic Culture Promotion Foundation, and Next Generation Leading Research Fund, and The Third Medium-Term Goals and Plans Fund of Kagawa University Research Promotion Program 2019 (KURPP).

Acknowledgments: We thank A. Sonoda at the Health Research Institute, AIST and N. Kusunose at Kagawa University for help with performing NMR measurements (A.S.) and DSC measurements (N.K.).

Conflicts of Interest: The authors declare no conflict of interest.

References

1. Adam, D.; Schuhmacher, P.; Simmerer, J.; Häußling, L.; Siemensmeyer, K.; Etbachi, K.H.; Ringsdorf, H.; Haarer, D. Fast photoconduction in the highly ordered columnar phase of a discotic liquid crystal. *Nature* **1994**, *371*, 141–143. [[CrossRef](#)]
2. Kumar, M. Self-organization of disc-like molecules: Chemical aspects. *Chem. Soc. Rev.* **2006**, *35*, 83–109. [[CrossRef](#)] [[PubMed](#)]
3. Laschat, S.; Baro, A.; Steinke, N.; Giesselmann, F.; Hägele, C.; Scalia, G.; Judele, R.; Kapatsina, E.; Sauer, S.; Schreivogel, A.; et al. Discotic liquid crystals: From tailor-made synthesis to plastic electronics. *Angew. Chem. Int. Ed.* **2007**, *46*, 4832–4887. [[CrossRef](#)]
4. Pisula, W.; Kastler, M.; Wasserfallen, D.; Mondeshki, M.; Piris, J.; Schnell, I.; Müllen, K. Relation between supramolecular order and charge carrier mobility of branched alkyl hexa-peri-hexabenzocoronenes. *Chem. Mater.* **2006**, *18*, 3634–3640. [[CrossRef](#)]
5. Sergeyev, S.; Pisula, W.; Geerts, Y.H. Discotic liquid crystals: A new generation of organic semiconductors. *Chem. Soc. Rev.* **2007**, *36*, 1902. [[CrossRef](#)]
6. Lemaure, V.; Filho, D.A.D.S.; Coropceanu, V.; Lehmann, M.; Geerts, Y.; Piris, J.; Debije, M.G.; van de Craats, A.M.; Senthilkumar, K.; Siebbeles, L.D.A.; et al. Charge transport properties in discotic liquid crystals: A quantum-chemical insight into structure–property relationships. *J. Am. Chem. Soc.* **2004**, *126*, 3271–3279. [[CrossRef](#)]
7. Crispin, X.; Cornil, J.; Friedlein, R.; Okudaira, K.K.; Lemaure, V.; Crispin, A.; Kestemont, G.; Lehmann, M.; Fahlman, M.; Lazzaroni, R.; et al. Electronic Delocalization in discotic liquid crystals: A joint experimental and theoretical study. *J. Am. Chem. Soc.* **2004**, *126*, 11889–11899. [[CrossRef](#)]
8. Lehmann, M.; Kestemont, G.; Aspe, R.G.; Buess-Herman, C.; Koch, M.H.J.; Debije, M.G.; Piris, J.; de Haas, M.P.; Warman, J.M.; Watson, M.D.; et al. High charge-carrier mobility in π -deficient discotic mesogens: Design and structure-property relationship. *Chem. Eur. J.* **2005**, *11*, 3349–3362. [[CrossRef](#)]
9. Roussel, O.; Kestemont, G.; Tant, J.; De Halleux, V.; Aspe, R.G.; Levin, J.; Remacle, A.; Gearba, I.R.; Ivanov, D.A.; Lehmann, M.; et al. Discotic liquid crystals as electron carrier materials. *Mol. Cryst. Liq. Cryst.* **2003**, *396*, 35–39. [[CrossRef](#)]
10. Ong, C.W.; Liao, S.-C.; Chang, T.H.; Hsu, H.-F. In situ synthesis of Hexakis(alkoxy)diquinoxalino [2,3-a:2',3'-c]phenazines: Mesogenic phase transition of the electron-deficient discotic compounds. *J. Org. Chem.* **2004**, *69*, 3181–3185. [[CrossRef](#)]
11. Yeh, M.-C.; Liao, S.-C.; Chao, S.-H.; Ong, C.W. Synthesis of polyphilic hexaazatrinaphthylenes and mesomorphic properties. *Tetrahedron* **2010**, *66*, 8888–8892. [[CrossRef](#)]
12. Kaafarani, B.R.; Kondo, T.; Yu, J.; Zhang, Q.; Dattilo, D.; Risko, C.; Jones, S.C.; Barlow, S.; Domercq, B.; Amy, F.; et al. High charge-carrier mobility in an amorphous hexaazatrinaphthylene derivative. *J. Am. Chem. Soc.* **2005**, *127*, 16358–16359. [[CrossRef](#)] [[PubMed](#)]
13. Budd, P.M.; Ghanem, B.; Msayib, K.; McKeown, N.; Tattershall, C. A nanoporous network polymer derived from hexaazatrinaphthylene with potential as an adsorbent and catalyst support. *J. Mater. Chem.* **2003**, *13*, 2721–2726. [[CrossRef](#)]
14. McKeown, N.; Gahnem, B.; Msayib, K.J.; Budd, P.M.; Tattershall, C.E.; Mahmood, K.; Tan, S.; Book, D.; Langmi, H.; Walton, A. Towards polymer-based hydrogen storage materials: Engineering ultramicroporous cavities within polymers of intrinsic microporosity. *Angew. Chem. Int. Ed.* **2006**, *45*, 1804–1807. [[CrossRef](#)] [[PubMed](#)]
15. Xu, F.; Chen, X.; Tang, Z.; Wu, D.; Fu, R.; Jiang, D. Redox-active conjugated microporous polymers: A new organic platform for highly efficient energy storage. *Chem. Commun.* **2014**, *50*, 4788–4790. [[CrossRef](#)]
16. Xiao, R.; Tobin, J.M.; Zha, M.; Hou, Y.-L.; He, J.; Vilela, F.; Xu, Z. A nanoporous graphene analog for superfast heavy metal removal and continuous-flow visible-light photoredox catalysis. *J. Mater. Chem. A* **2017**, *5*, 20180–20187. [[CrossRef](#)]
17. Hisaki, I.; Suzuki, Y.; Gomez, E.; Ji, Q.; Tohnai, N.; Nakamura, T.; Douhal, A. Acid responsive hydrogen-bonded organic frameworks. *J. Am. Chem. Soc.* **2019**, *141*, 2111–2121. [[CrossRef](#)]
18. Bradshaw, J.S.; Izatt, R. Crown ethers: The search for selective ion ligating agents. *Acc. Chem. Res.* **1997**, *30*, 338–345. [[CrossRef](#)]

19. Isoda, K. Acid-responsive N-heteroacene-based material showing multi-emission colors. *ChemistryOpen* **2017**, *6*, 242–246. [[CrossRef](#)]
20. Isoda, K.; Sato, Y.; Matsukuma, D. Fluorescent N-heteroacene-based π -conjugated liquid responsive to HCl vapor. *ChemistrySelect* **2017**, *2*, 7222–7226. [[CrossRef](#)]
21. Sato, Y.; Mutoh, Y.; Matsukuma, D.; Nakagawa, M.; Kawai, T.; Isoda, K. Tuning the electronic properties and acid-response behavior of N-heteroacene-based π -conjugated liquids by changing the number of π -conjugated substituents. *Chem. Asian J.* **2018**, *13*, 2619–2625. [[CrossRef](#)] [[PubMed](#)]
22. Isoda, K.; Ikenaga, A. Synthesis of furan-substituted N-heteroacene-based liquid material and its acid-recognizing behavior. *Crystals* **2019**, *9*, 51. [[CrossRef](#)]
23. Isoda, K.; Ishiyama, T.; Mutoh, Y.; Matsukuma, D. Stimuli-responsive room-temperature N-heteroacene liquid: In situ observation of the self-assembling process and its multiple properties. *ACS Appl. Mater. Interfaces* **2019**, *11*, 12053–12062. [[CrossRef](#)] [[PubMed](#)]
24. Isoda, K.; Matsubara, M.; Ikenaga, A.; Akiyama, Y.; Mutoh, Y. Reversibly/irreversibly stimuli-responsive inks based on N-heteroacene liquids. *J. Mater. Chem. C* **2019**, *7*, 14075–14079. [[CrossRef](#)]
25. Hariharan, P.; Pople, J. The effect of d-functions on molecular orbital energies for hydrocarbons. *Chem. Phys. Lett.* **1972**, *16*, 217–219. [[CrossRef](#)]
26. Hariharan, P.C.; Pople, J.A. The influence of polarization functions on molecular orbital hydrogenation energies. *Theor. Chim. Acta* **1973**, *28*, 213–222. [[CrossRef](#)]
27. Lee, C.; Yang, W.; Parr, R.G. Development of the Colle-Salvetti correlation-energy formula into a functional of the electron density. *Phys. Rev. B* **1988**, *37*, 785–789. [[CrossRef](#)]
28. Isoda, K.; Takahashi, H.; Mutoh, Y.; Hoshino, N.; Akutagawa, T.; Hoshino, T. One-dimensional single-helix coordination polymer self-assembled by a crown-ether appended-N-heteroacene radical anion. *Dalton Trans.* **2019**, *48*, 13125–13129. [[CrossRef](#)]
29. Isoda, K.; Abe, T.; Tadokoro, M. Room-temperature redox-active liquid crystals composed of tetraazanaphthacene derivatives. *Chem. Asian J.* **2013**, *8*, 2951–2954. [[CrossRef](#)]



© 2020 by the authors. Licensee MDPI, Basel, Switzerland. This article is an open access article distributed under the terms and conditions of the Creative Commons Attribution (CC BY) license (<http://creativecommons.org/licenses/by/4.0/>).